Journal of Power Sources 196 (2011) 3766–3772

Contents lists available at ScienceDirect

Journal of Power Sources

journal homepage: www.elsevier.com/locate/jpowsour

# Development of a novel pseudo bipolar piezoelectric proton exchange membrane fuel cell with nozzle and diffuser

Hsiao-Kang Ma*, Jyun-Sheng Wang, Ya-Ting Chang

*Department of Mechanical Engineering, National Taiwan University, No. 1, Roosevelt Road, Section 4, Taipei 10617, Taiwan, ROC*

ARTICLE INFO

*Article history:*
Received 11 December 2010
Accepted 17 December 2010
Available online 8 January 2011

*Keywords:*
Piezoelectric
Fuel cell
Nozzle
Diffuser
Air-breathing
Pseudo bipolar design

ABSTRACT

Previous studies of a piezoelectric proton exchange membrane fuel cell with nozzle and diffuser (PZT-PEMFC-ND) have shown that a PZT device could solve the cathode flooding problems and improve cell performance. In this study, an innovative design for a PZT-PEMFC-ND bi-cell with pseudo bipolar electrodes is developed to achieve a higher power in the stack design to solve water-flooding problems and improve cell performance. This new design, with a reaction area of 8 $cm^2$, contains two cells with two outside anodes and two inside cathodes that share a common PZT vibrating device for pumping air flow. The influence of the varying aspect ratio (AR) of the diffuser elements on the unit cell-flow rate is investigated using a three-dimensional transitional model. The simulation results show that a proper AR value of 11.25 for the diffuser, with a smaller diffuser angle of 5°, could ensure a smoother intake of the air and, thus, better cell performance. The experimental results show that the performance of the PZT-PEMFC-ND bi-cell can be 1.6 times greater than that of the single cell.



## 1. Introduction

Air-breathing proton exchange membrane fuel cells (AB-PEMFCs) have attracted attention for their potential as a power source for low power portable electronic devices. AB-PEMFCs are characterized by a simple structure and a minimum balance of plant, due to their need for fewer auxiliary requirements to support PEMFC performance, such as compressors, humidifiers, and heat exchangers. They could be (1) passively supplied with air by natural convection alone, or (2) actively supplied with air using an additional oxygen supply device. In the former case, the chemical reactions mainly depend upon natural convection, caused by temperature and oxygen concentration gradients. In order to deliver sufficient oxygen into the cathode chamber, in the latter case, an open-air cathode PEMFC stack, with a fan as the oxygen supplier, was proposed [1]. In addition, dehydrating phenomena slightly influenced the performance of the AB-PEMFCs [2]. Catalyst loading, relative humidity, temperature, hydrogen stoichiometry, gas-diffusion layer thickness, and cathode structure are important parameters in the performance of AB-PEMFCs [3,4].

During the AB-PEMFC operation, liquid water was transported by electro-osmotic drag, back diffusion from the cathode, pressure-driven hydraulic permeation, thermal-osmotic drag, and diffusion between the flow stream and the membrane [5]. The net electro-osmotic drag coefficient was found to be a function of the water content of the membrane and temperature [6,7]. Generally, the net electro-osmotic drag coefficient increases as water content increases in the membrane. At a high water content, the net electro-osmotic drag coefficient increased as the temperature increased. Yi and Nguyen [8] showed that PEMFC performance was improved by anode humidification and positive differential pressure between the cathode and anode, which is also proved by the Nernst equation. Thus, water transport and management depend upon the structure and properties of the cell components, the reactant stream humidification, the flow field layout, and the structural and wetting properties of the gas diffusion media and micro porous layer [9].

Over the past several years, various PEMFC stacks have been developed according to differing considerations of functional demands and system designs. Depending upon differences in the electrode units in the stack design, the major types of PEMFC stacks are classified as bipolar, monopolar, and pseudo bipolar [10]. The bipolar design has been the most common type used in PEMFCs over the years due to its advantages, such as its compact volume, its low internal resistance, and its ability to operate at high pressure. However, the manufacturing cost is high and the bipolar plate design is complex. Although the bipolar design can produce a high power, water and thermal management play important roles in its performance. Among types of PEMFC stacks, the monopolar design is suitable for applications in a low power and high voltage system. However, the monopolar design is characterized by its high resistance and performance, which significantly depends

* Corresponding author. Tel.: +886 2 23629976; fax: +886 2 23632644.
*E-mail address:* skma@ntu.edu.tw (H.-K. Ma).

0378-7753/$ – see front matter © 2011 Elsevier B.V. All rights reserved.
doi:10.1016/j.jpowsour.2010.12.093

**Nomenclature**

| | |
|---|---|
| $A_{PZT}$ | piezoelectric area ($m^2$) |
| $AR$ | aspect ratio |
| $C$ | conductivity coefficient |
| $D$ | channel opening width |
| $f$ | frequency of PZT (Hz) |
| $L$ | channel path |
| $P$ | pressure ($N\,m^{-2}$) |
| $P_c$ | channel pressure |
| $P_{in}$ | inlet pressure |
| $P_{out}$ | outlet pressure |
| $R$ | gas constant ($J\,mol^{-1}\,K^{-1}$) |
| $t$ | time (s) |
| $T$ | temperature (°C) |
| $V_{PZT}$ | motion equation of the piezoelectric device ($m\,s^{-1}$) |
| $Q$ | flow rate |
| $\xi$ | loss coefficient |
| $\theta$ | diffuser angle |
| $\rho$ | density ($kg\,m^{-3}$) |

upon the operational temperature and the humidity in the surrounding area. The traditional pseudo bipolar design, as shown in Fig. 1, contains two cells with two inside anodes and two outside cathodes. Although it was necessary to link each bi-cell, electrically, to obtain higher voltage, thermal management was easy with a parasitic power such as an air fan or blower [11].

For portable application of a PEMFC, the air supply device should be small in size, provide enough airflow, and require low power consumption. Various actuating methods, such as electrostatic, magnetostriction, shape memory alloy, thermopneumatic, and piezoelectric, have been developed to pump fluid in a precise manner. Among these actuating methods, the piezoelectric concept shows good reliability, energy efficiency, and moderate volume displacement [12]. To improve the pumping flow rate, Olsson [13], Ullmann [14], and Yang [15] have investigated the piezoelectric valveless micropump system with two chambers arranged in series or parallel. The results show that the flow rate could be controlled by changing the phase difference. At a phase angle of 90°, an eight-fold increase of flow rate for a series arrangement is seen relative to that of a single-chamber operation. Furthermore, for a parallel arrangement, the flow rate is less than that of a series arrangement.

Previous studies [16–18] indicated that a novel design for proton exchange membrane fuel cells with a piezoelectric device (PZT-PEMFC), which is an actuator for pumping air into the cathode chamber, offers better performance with higher current generation. These simulation results indicate that a PZT-PEMFC can compress more air into the catalyst layer and, thus, enhance electrochemical reactions, resulting in higher current output. At the same time, water vapor is pumped from the cathode chamber. The experimental study of a piezoelectric proton exchange membrane fuel

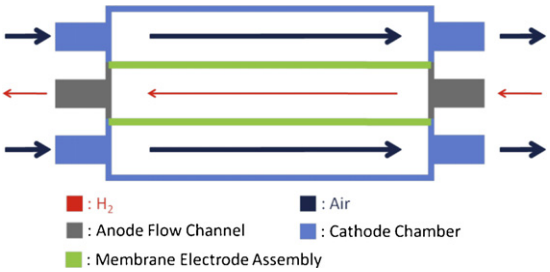


**Fig. 1.** The traditional pseudo bipolar design.

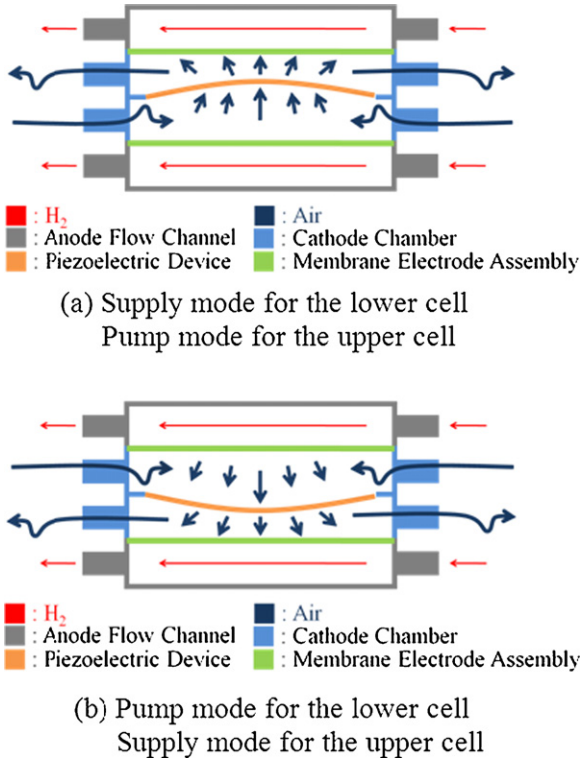


**Fig. 2.** Operation modes of the novel pseudo bipolar design of PZT-PEMFC-ND bi-cell.

cell with nozzle and diffuser, called a PZT-PEMFC-ND, proved that the PZT device could solve water-flooding problems and improve cell performance [19]. The results also showed that a better PZT-PEMFC-ND cell performance was obtained under a higher aspect ratio (AR) of 11.25 at the diffuser angle ($\theta$) of 22.89°. The aspect ratio is defined as the cathode channel path divided by the channel opening width. Previous studies indicated that the rectification efficiency of the diffuser elements ($\gamma$), the PZT vibrating frequency ($f$), and the displaced volume per stroke ($\Delta V$) affected the flow rate of the PZT device. The rectification efficiency is defined as the net flow rate over the displaced volume per stroke and, thus, conceived as an indicator of the preferential direction. Its value depends upon the geometrical parameters (AR and $\theta$) and the Reynolds number [20].

The objective of this study is to develop a PZT-PEMFC-ND bi-cell with a novel pseudo bipolar design and to investigate its performance. The experimental parameters include PZT vibration frequency, cell operation temperature, current density, and the nozzle and diffuser designs. A 3D transitional model, based on the semi-implicit method for pressure line equations consistent (SIMPLEC) procedure, was used to analyze the effects of the diffuser geometry on the flow behavior of the PZT-PEMFC-ND.

## 2. The novel pseudo bipolar design of the air-breathing PZT-PEMFC-ND

### 2.1. Actuation mechanism

In this study, the PZT-PEMFC-ND bi-cell was constructed using a novel pseudo bipolar design to deliver higher power. This design differs from the traditional pseudo bipolar design, in that, in the traditional pseudo bipolar design, the cathodes are outside the cell. However, the novel pseudo bipolar design consisted of two cells, with two outside anodes and two inside cathodes that shared a common PZT vibrating device to pump airflow, as shown in Fig. 2.

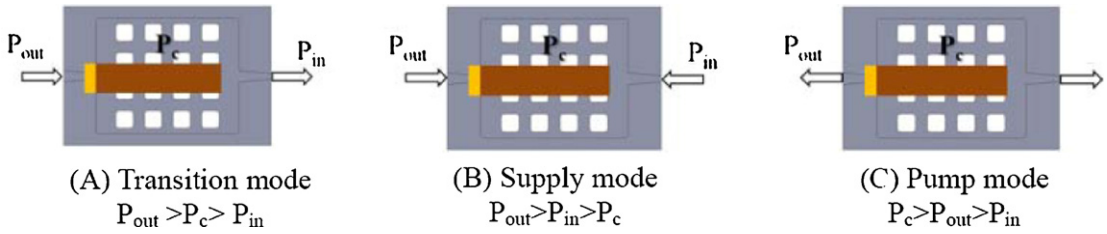


**Fig. 3.** The flow modes during the pumping process.

This arrangement allows one PZT device to supply air into the two cells and pump out the produced water, saving the power consumption of the air supply device. Fig. 2 shows the mechanism of the novel pseudo bipolar design of the PZT-PEMFC-ND bi-cell module operated in supply mode and pump mode. When one cell is operated in supply mode, sucking air into the cathode, the other cell is in pump mode, delivering reacted gas and produced water out of the cathode chamber. Placing the PZT device between the two cathodes resulted in the operation modes of the two cells being opposite. The phase difference was just a half of the period. This means that when one cell operates at the supply mode and delivers a higher current output, the other operates at the pump mode and delivers a lower current output. In previous studies [16–19], the results showed that using a higher frequency can lead to a more stable current output.

### 2.2. Flow mode analysis

The lumped system developed by Ullmann [14] was applied to understand the characteristics of the valveless PZT pumping system. This method neglected the spatial variations and focused on the time variations, which do not need complex CFD methods, such as Navier–Stokes equations. The method was carried out for the following three regions as shown in Fig. 3: pump mode ($P_c > P_{out} > P_{in}$), supply mode ($P_{out} > P_{in} > P_c$), and transition mode ($P_{out} > P_c > P_{in}$). An assumption was made that the inlet pressure, $P_{in}$, was always smaller than the outlet pressure, $P_{out}$, due to the nozzle/diffuser design. In supply mode, the diaphragm moved outward and the cathode chamber volume increased, which caused the chamber pressure to become lower than the atmospheric pressure and, thus, the air was sucked into the chamber. In pump mode, the diaphragm moved inward and the cathode chamber volume decreased. Because the pressure inside the cell was higher than the atmospheric pressure, the air was pushed into the catalyst layer and the water produced was pumped out of the cell. A transition mode occurred between the pump mode and the supply mode, when the outlet pressure was higher than the chamber and inlet pressures, $P_{out} > P_c > P_{in}$. This method may validate the nozzle/diffuser designs and compared them with the CFD method [21].

In this study, a three-dimensional transitional model, based on the semi-implicit method for pressure line equations consistent (SIMPLEC) procedure, was used to analyze the effects of the diffuser geometry on the flow behavior of the PZT-PEMFC-ND. The assumptions are as follows:

(1) The air is treated as ideal gases.
(2) The Stefan–Maxwell equations are applied to multispecies diffusion.
(3) The porosity and permeability of the porous media are uniform, and the porous media are isotropic and homogeneous.
(4) The effect of gravity is ignored.
(5) The amplitude of the PZT device is assumed constant, and the motion of PZT device is assumed to be a sine function.
(6) The structure of the bi-cell is assumed to be symmetric.

The fluid driving forces at the anode and cathode inlets differed in the PZT-PEMFC-ND systems. The hydrogen was supplied from a hydrogen storage bottle, and the hydrogen flow rate was controlled by a mass flow controller. In the experimental study, the hydrogen-volume flow rate was always a constant, at 30 ml $min^{-1}$ for each cell. On the other hand, the airflow to the cathode was driven by PZT vibrations.

To analyze the airflow rate of the PZT-PEMFC-ND system, the control volume of the system was chosen in the cathode chamber (Fig. 4). The equation of motion for the PZT device was a sine function given by Eq. (1):

$$\vec{V}_{PZT} = \frac{d}{dt}\left[-0.00025 \times (\sin(2\pi f t))\right] \quad (1)$$

where $\vec{V}_{PZT}$ is the vibration velocity (m $s^{-1}$) of the PZT material, $f$ is the frequency (Hz), and $t$ represents the time (s).

The inflow and outflow periods in the chamber were induced by the sine function. By using the Reynolds transport theorem and the continuity equation [16–19], the cathode flow rate can be written as:

$$Q_c = \frac{1}{r}\frac{\partial}{\partial t}\int_{CV}\frac{P}{T}d\forall + \rho\vec{V}_{PZT}A_{PZT} \quad (2)$$

and the volume change rate can be written as Eq. (3):

$$\frac{d\forall}{dt} = 2\pi f \forall_0 \sin(2\pi f) - \forall_0\left[\frac{(dp/dt)}{P_b - P_{atm}}\right] \quad (3)$$

where the blocking pressure, $P_b$, is associated with the stiffness of the diaphragm.

It has been proven that a PZT-PEMFC-ND single cell can supply air into the cathode chamber and solve the water-flooding problem. However, the geometrical parameters of the diffuser, including the diffuser angle ($\theta$), the channel path ($L$), and the channel opening width ($D$), shown in Fig. 5, affect cell performance. To achieve high actuation pressures, smaller diffuser angles should be utilized in order to approach the maximum rectification effect of the diffuser. The aspect ratio influences the rectification effect, as well. A previous study [19] indicated that a larger aspect ratio at the diffuser angle of 21–23° should be chosen to achieve higher actuation pressure.

The diffuser element theory can be applied to the airflow rate in the cathode chamber of the PZT-PEMFC-ND. The inlet flow rate

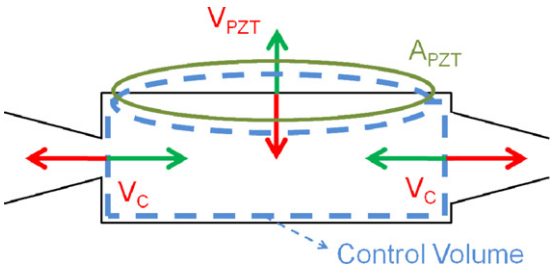


**Fig. 4.** The diagram of control volume in a PZT-PEMFC-ND.

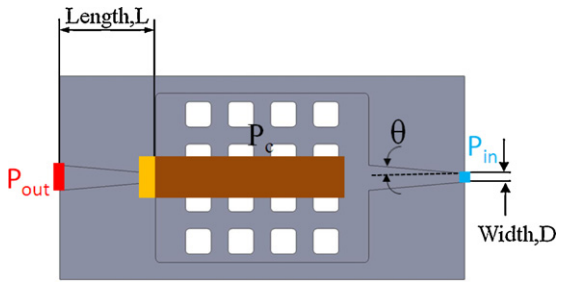


**Fig. 5.** The cathode chamber design of a PZT-PEMFC-ND.

can be found by using the continuity equation as follows:

$$Q_{\text{in},l} = C_{\text{n}}\sqrt{(P_{\text{out}} - P_{\text{c}})} \tag{4}$$

for the air inflow from left to right, shown in Fig. 4

$$Q_{\text{in},r} = C_{\text{d}}\sqrt{(P_{\text{in}} - P_{\text{c}})} \tag{5}$$

for the air inflow from right to left, shown in Fig. 4

The conductivity coefficient can be separated into nozzle, $C_{\text{n}}$, and diffuser, $C_{\text{d}}$.

$$C_{\text{n}} = \frac{A}{\sqrt{1/2(\xi_{\text{n}}\rho)}} \tag{6}$$

$$C_{\text{d}} = \frac{A}{\sqrt{1/2(\xi_{\text{d}}\rho)}} \tag{7}$$

where $\xi_{\text{n}}$ and $\xi_{\text{d}}$ are the loss coefficients for the nozzle and diffuser, respectively.

In the supply mode, the loss coefficient for the nozzle is smaller than that of the diffuser and, thus, induces a larger airflow rate from the nozzle into the cathode chamber. Although the net flow rate can be calculated using this method, the outflow rate is irrelevant to this study. The major reason for this is that the air through the outlet reacted throughout the electrochemical reaction.

## 3. Experimental setup

Fig. 6 shows the test platform for analyzing the performance of a PZT-PEMFC-ND module. On the anode side, the hydrogen from the hydrogen storage bottle flows through the mass flow controller and enters the bubble humidifier. The humidifier is a water tank with a heater that allows the reactant gas to pass through at a specific temperature. Next, the hydrogen with water vapor is delivered to the PZT-PEMFC-ND module for an electrochemical reaction. To activate the PZT vibrating device, a function generator is utilized, first, to deliver the sine wave signals, then the signals from the function generator are sent to an amplifier to magnify the signals so that the piezoelectric device vibrates when it receives the signal. To measure the power consumption of the PZT device, a power meter is connected to the output terminal of the amplifier.

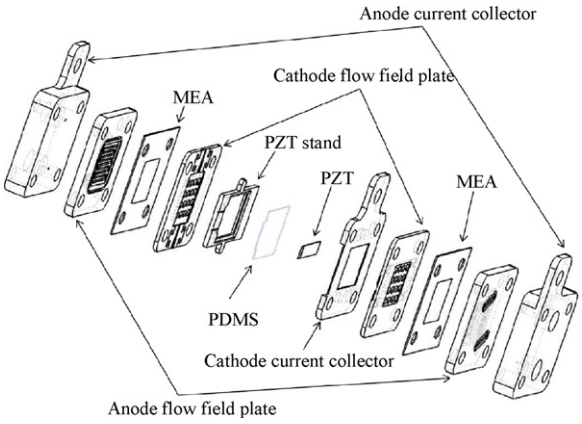


**Fig. 7.** An exploded drawing of the PZT-PEMFC bi-cell.

The PZT-PEMFC-ND bi-cell, shown in Fig. 7, consists of two anode current collectors, two anode flow-field plates, two membrane electrode assemblies (MEA), one PZT device, and one PZT stand. The reaction area of the MEA is $2 \times 2\,\text{cm}^2$ for each single cell, the membrane is Nafion®212, and the opening ratio is 34.7% in the cathode. The PZT material is attached to a gasket film, made of PDMS, on the PZT stand to prevent gas leakage and to increase the volume change of the cathode chamber. Fig. 8 shows the assembled single cell, the bi-cell, and the setup of the bi-cell experiment. In this study, the two cells were electrically parallel and, thus, the reaction area for the bi-cell is $8\,\text{cm}^2$. As a result, two hydrogen supply lines and two thermocouples were prepared. In contrast, the signal from the amplifier was transmitted through the signal wires in the middle of the module.

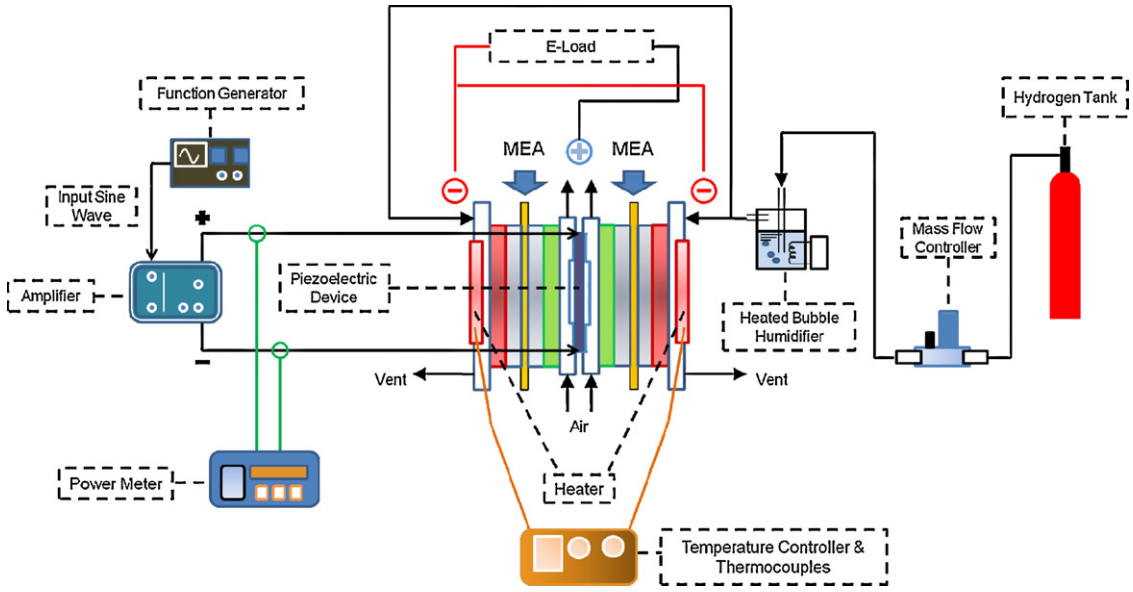


**Fig. 6.** Schematic of the PZT-PEMFC testing system.

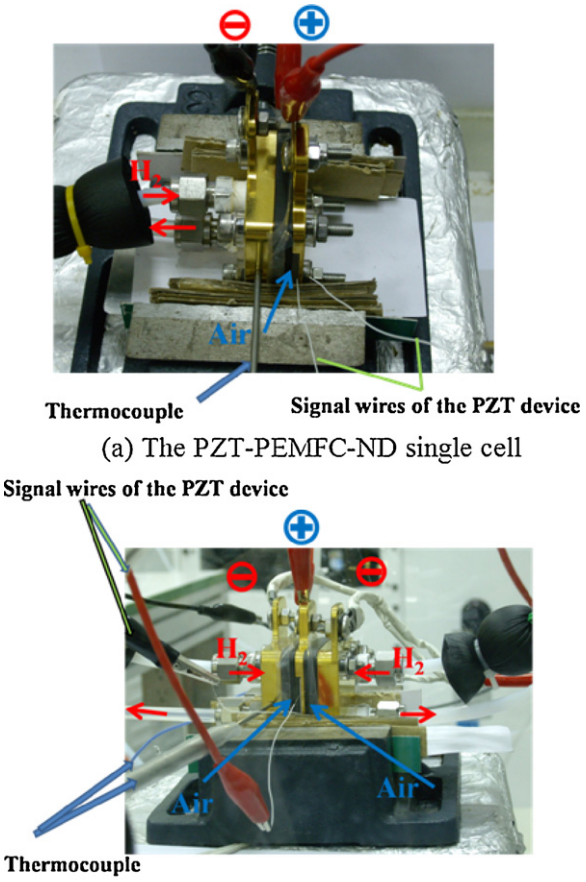


**Fig. 8.** Experimental setup of the PZT-PEMFC-ND single cell and bi-cell.

The PZT device of the PZT-PEMFC-ND was driven by a sine wave signal generated by a function generator. The amplifier was required to magnify voltage to the designated dB. The vibration frequency of the PZT device shifted from 120 Hz to 210 Hz; thus, the PZT device controlled the airflow on the cathode side. The ambient condition is considered at environmental temperature 27 °C and relative humidity 47%. On the anode side, the humidified hydrogen, at a temperature of 30–50° C, flowed into the anode channel. The hydrogen in the anode side was supplied by hydrogen storage and controlled by the mass flow controller at 30 ml $min^{-1}$ for each cell. The DC electronic load simulated the electronic loading of voltage and current. In this study, a constant voltage mode was chosen, and the polarization curves were obtained by decreasing 0.1 V from an open circuit voltage to 0.3 V every 10 min using LabVIEW software.

## 4. Results and discussion

In this study, the influence of the operating temperature, PZT vibrating frequency, and the aspect ratio at a smaller angle 5° were investigated to achieve higher performance for the PZT-PEMFC-ND single cell. These parameters were, then, applied to a bi-cell to compare the performance of the PZT-PEMFC-ND single cell and the bi-cell, using the novel pseudo bipolar design.

### 4.1. Influence of PZT vibration frequencies

A previous study [19] indicated that the PZT-PEMFC-ND single cell operated under the PZT vibration frequency of 180 Hz, using a larger diffuser angle of 22.89° and an aspect ratio of 11.25. This single cell could achieve the same performance as the open cathode

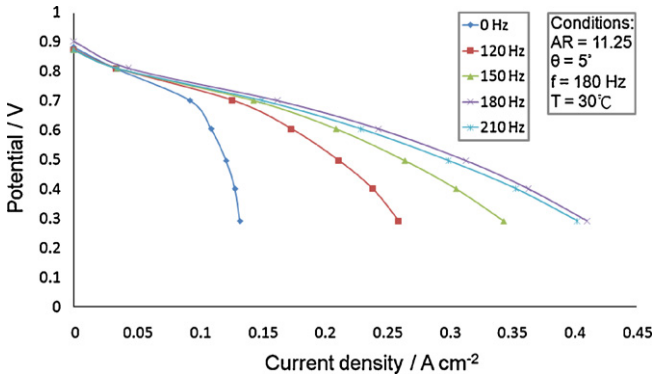


**Fig. 9.** The *I–V* curves under different PZT vibration frequencies at $T = 30\,^{\circ}C$, AR = 11.25 and $\theta = 5^{\circ}$.

case without a fan. The actuation force of the fluid motion depends upon the PZT material, the chamber size, and the PZT vibration frequency. While the designed PZT device is operated at a harmonic frequency, the cell performance can be improved by sucking more air into the chamber and pumping more water out. In this study, a diffuser with a smaller angle of 5° was utilized to attain higher actuation pressure. Fig. 9 shows the performance of a PZT-PEMFC-ND single cell operated under different PZT vibration frequencies at 30 °C. The results showed that the performances increased with frequency, increasing from $f = 120$ Hz to $f = 180$ Hz, because more air was sucked in and more water was pumped out on the cathode side, thereby improving the performance. The maximum current reached 0.41 A at $f = 180$ Hz, which was almost three times greater than the case without PZT vibration ($f = 0$ Hz). A higher operating frequency may reach another harmonic resonance of the design and result in a higher performance, but the lifetime of the PZT material would be greatly shortened. Thus, the results show that in this study the optimal PZT vibration frequency is 180 Hz for the PZT-PEMFC-ND single cell with a smaller diffuser angle of 5°.

### 4.2. Influence of operation temperature

A previous study [11] has shown that the proper operation temperature of an AB-PEMFC with pseudo bipolar design would be from 20 °C to 40 °C and the hydrogen flow rate would not have an apparent effect on the performance. Furthermore, the performance of the AB-PEMFC with a pseudo bipolar design was affected by the humidity in the surroundings and the operational temperature. Previous studies [22,23] also indicated that an appropriate increase in cell temperature is an important parameter to ensure high cell performance.

Fig. 10 shows the *I–V* curves at different temperatures under a PZT vibration frequency of 180 Hz. As the temperature increases

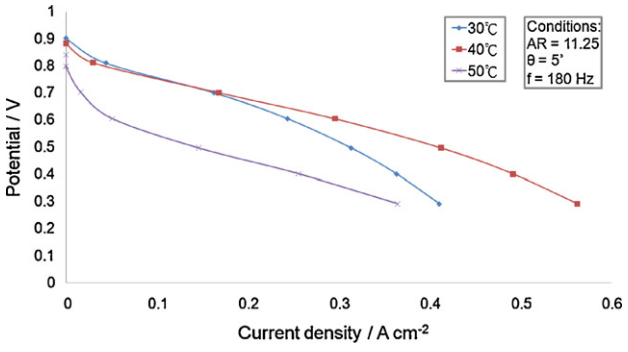


**Fig. 10.** *I–V* curves under different operation temperatures at $f = 180$ Hz, AR = 11.25 and $\theta = 5^{\circ}$.

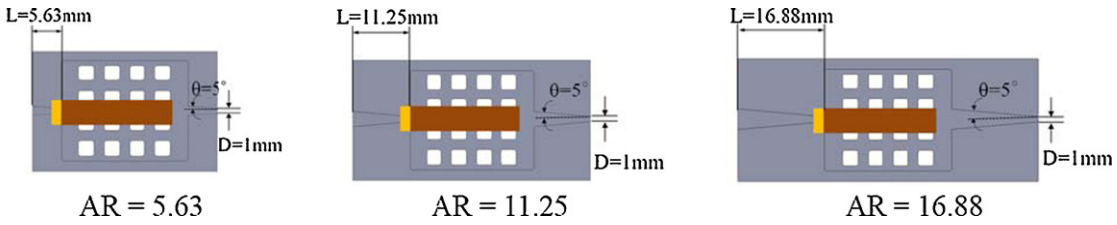


**Fig. 11.** Different diffuser designs of the PZT-PEMFC-ND module.

from 30 °C to 40 °C, the current output and cell performance increases because a high cell temperature improves the chemical reaction rate. Thus, more water is generated to hydrate the membrane and the ohmic loss is decreased. In addition, the current density and cell performance decrease as temperature increases from 40 °C to 50 °C because a larger activation loss was induced at the higher temperature. More water vaporized at the higher temperature, thus the membrane dries out and then lowers the membrane conductivity. In the ohmic loss region, this condition may be recovered by back diffusion from the cathode. The results indicate that a PZT-PEMFC-ND single cell with a smaller $\theta$ of 5° should operate at a proper temperature of 40 °C to reach the balance of water transport.

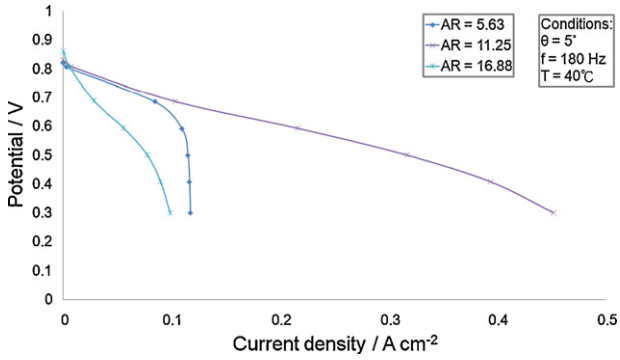


**Fig. 12.** *I–V* curves under different aspect ratios in the PZT-PEMFC-ND at $T$ = 40 °C, $f$ = 180 Hz and $\theta$ = 5°.

### 4.3. Influence of aspect ratio

The pump performance of the PZT-PEMFC-ND module is a function of geometry parameters: aspect ratio (AR) and diffuser angle ($\theta$). A previous study [19] revealed that the PZT-PEMFC-ND single cell, using a larger AR of 11.25 at a larger $\theta$ of 22.89°, could achieve a better performance. In this study, the performances under different aspect ratios at a smaller $\theta$ of 5° were investigated. Fig. 11 shows the different diffuser design in the PZT-PEMFC-ND module. The diffuser angle is fixed at 5° and the channel opening width is 1 mm for different AR, so the channel length is equal to the aspect ratio.

Fig. 12 indicates that the *I–V* curves do not improve continuously when the aspect ratio increases. For a lower aspect ratio of 5.63, the *I–V* curves dropped in the regions of concentration losses. This is because the pressure difference between the cathode chamber and the surroundings was not strong enough. In Fig. 13, insufficient air was sucked into the chamber and, thus, the produced water could not be pumped out. However, for a higher aspect ratio of 16.88, the performance did not improve, although the pressure difference was larger than it was in the other cases. The reason for this is that the blocking phenomenon occurred inside the diffuser element. Fig. 14 shows the detailed velocity profile of different aspect ratios in the supply mode. In the supply mode, the flows from the nozzle and diffuser collide in the cathode chamber, and then result in a larger pressure in the chamber. When the aspect ratio increased, the velocity from the nozzle was larger than that from the diffuser, so the point of collision moved toward the diffuser. For the aspect

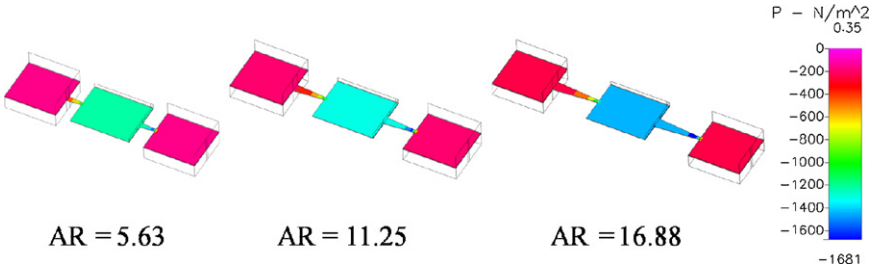


**Fig. 13.** Pressure distributions under different aspect ratios at $\theta$ = 5° in the PZT-PEMFC-ND single cell ($f$ = 180 Hz, $t$ = 1 s).

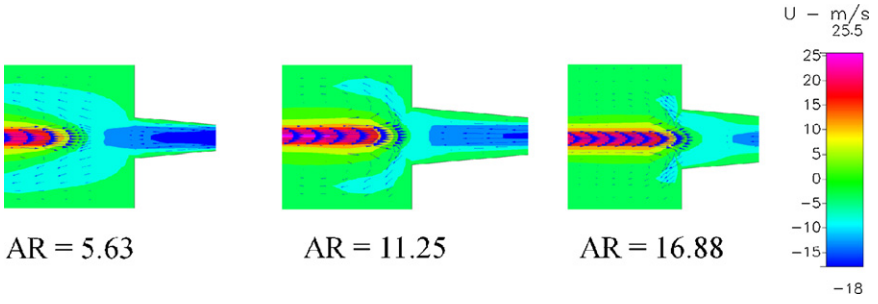


**Fig. 14.** Velocity profiles under different aspect ratios at $\theta$ = 5° in the PZT-PEMFC-ND single cell ($f$ = 180 Hz, $t$ = 1 s).

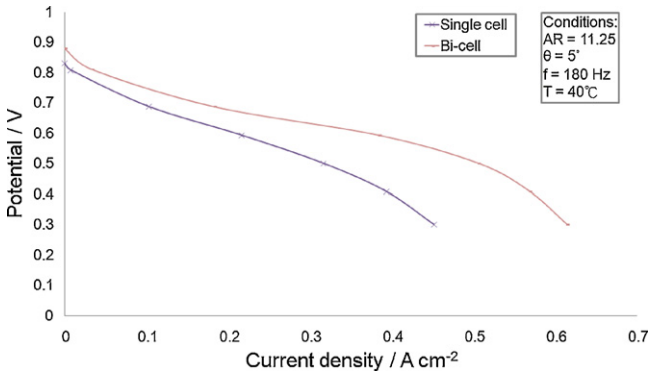


**Fig. 15.** *I–V* curves of the PZT-PEMFC-ND single cell and bi-cell.

ratio of 16.88, this collision point sat inside the diffuser element and the blocking phenomenon occurred. Thus, the flow from the diffuser into the cathode chamber was obstructed and less air was sucked into the cathode chamber. As a result, the optimal aspect ratio is 11.25 at the diffuser angle 5° in this study.

### 4.4. Performance of PZT-PEMFC-ND bi-cell

In this study, the optimal operation parameters of the PZT-PEMFC-ND single cell are the aspect ratio of 11.25, the diffuser angle of 5°, PZT vibration frequency of 180 Hz, and the operation temperature of 40 °C. Fig. 15 compares the performances of the PZT-PEMFC-ND single cell and bi-cell using a novel pseudo bipolar design when these parameters are applied. The results show that the ohmic loss was smaller when the module was operated in the bi-cell mode. The PZT-PEMFC-ND single cell and bi-cell generated 0.64 W and 1 W, respectively. As a result, the bi-cell performed 1.6 times better than the single cell. The reason why the performance was not twice that of the single cell may be due to the slight water condensation found in the anode flow channels of one cell after examination of the module's interior. This was probably due to the back diffusion of the liquid water from the cathode, since the condensation phenomena were not found in the cathode. This condition could be reduced by increasing the hydrogen flow rate or lowering the inlet humidity.

### 4.5. Required power of PZT-PEMFC-ND bi-cell

The novel pseudo bipolar design of the PZT-PEMFC-ND module could operate in single cell or bi-cell mode, and only one PZT device is required for the module. The module can be installed with a DC–AC inverter to invert the DC voltage into a higher AC voltage, such as 50–150 V. In this study, the PZT-PEMFC-ND bi-cell generates 1 W at $T = 40\,^{\circ}C$, $f = 180$ Hz, AR = 11.25, and $\theta = 5^{\circ}$. The PZT device is a power-consuming device and requires about 0.2 W when it is operated at 180 Hz using 100 V, so the net power output of the bi-cell is about 0.8 W.

## 5. Conclusion

A novel pseudo bipolar design for the PZT-PEMFC-ND bi-cell has been successfully developed. The mechanism of the PZT-PEMFC-ND bi-cell has been proposed in three different flow modes. The major findings are as follows:

(1) The PZT vibration frequency and cell temperature are the important operating parameters for increasing the performance of the PZT-PEMFC-ND module. The optimal PZT vibration frequency is $f = 180$ Hz at a temperature of 40 °C.
(2) The performance of the PZT-PEMFC-ND module would be restricted by the blocking phenomenon induced by a larger aspect ratio. The optimal geometry parameters are AR at 11.25 under $\theta = 5^{\circ}$.
(3) The PZT-PEMFC-ND bi-cell generates 1 W at $T = 40\,^{\circ}C$, $f = 180$ Hz, AR = 11.25, and $\theta = 5^{\circ}$. When compared with the single cell, the performance of the PZT-PEMFC-ND bi-cell was 1.6 times greater. The net power output of the bi-cell is about 0.8 W, due to the power consumption of 0.2 W for the PZT device at 180 Hz.
(4) The novel pseudo bipolar design of PZT-PEMFC-ND may be applied on a stack to improve water management.

## Acknowledgement

This research was funded by the National Science Council of the Republic of China (NSC 99-2221-E-002-126-MY2).

## References

[1] D.T. Santa Rosa, D.G. Pinto, V.S. Silva, R.A. Silva, C.M. Rangel, Int. J. Hydrogen Energy 32 (2007) 4350–4357.
[2] L. Matamoros, D. Bruggemann, J. Power Sources 173 (2007) 367–374.
[3] S.U. Jeong, E.A. Cho, H.J. Kim, T.K. Lim, I.H. Oh, S.H. Kim, J. Power Sources 159 (2006) 1089–1094.
[4] S.U. Jeong, E.A. Cho, H.J. Kim, T.K. Lim, I.H. Oh, S.H. Kim, J. Power Sources 158 (2006) 348–353.
[5] W. Dai, H. Wang, X.-Z. Yuan, J.J. Martin, D. Yang, J. Qiao, J. Ma., Int. J. Hydrogen Energy 34 (2009) 9461–9478.
[6] T.F. Fuller, J. Newman, J. Electrochem. Soc. 139 (1992) 1332–1337.
[7] S.H. Ge, B.L. Yi, P.W. Ming, J. Electrochem. Soc. 153 (2006) A1443–A1450.
[8] J.S. Yi, T.V. Nguyen, J. Electrochem. Soc. 145 (1998) 1149–1159.
[9] H. Li, Y. Tang, Z. Wang, Z. Shi, S. Wu, D. Song, J. Zhang, K. Fatih, J. Zhang, H. Wang, Z. Liu, R. Abouatallah, A. Mazza, J. Power Sources 178 (2008) 103–117.
[10] R. Jiang, D. Chu, J. Power Sources 93 (2001) 25–31.
[11] D. Chu, R. Jiang, J. Power Sources 83 (1999) 128–133.
[12] X. Yang, Z. Zhou, H. Cho, X. Luo, Sens. Actuators A 130–131 (2006) 531–536.
[13] A. Olsson, G. Stemme, E. Stemme, Sens. Actuators A 47 (1995) 549–556.
[14] A. Ullmann, Sens. Actuators A 69 (1998) 97–105.
[15] K.-S. Yang, I.-Y. Chen, C.-C. Wang, Chem. Eng. Technol. 29 (2006) 703–710.
[16] H.-K. Ma, S.-H. Huang, B.-R. Chen, L.-W. Cheng, J. Power Sources 180 (2008) 402–409.
[17] H.-K. Ma, S.-H. Huang, Y.-Z. Kuo, J. Power Sources 185 (2008) 1154–1161.
[18] H.-K. Ma, S.-H. Huang, J. Fuel Cell Sci. Technol. 6 (2009) 034501-1–034501-6.
[19] H.-K. Ma, S.-H. Huang, J.-S. Wang, C.-G. Hou, C.-C. Yu, B.-R. Chen, J. Power Sources 195 (2010) 1393–1400.
[20] M. Ahmadian, A. Mhrabian, J. Phys. 34 (2006) 379–384.
[21] Y.-Y. Tsui, S.-L. Lu, Sens. Actuators A 148 (2008) 138–148.
[22] J.-H. Jang, H.-C. Chiu, W.-M. Yan, W.-L. Sun, J. Power Sources 180 (2008) 476–483.
[23] W.-M. Yan, X.-D. Wang, S.-S. Mei, X.-F. Peng, Y.-F. Guo, A. Su, J. Power Sources 185 (2008) 1040–1048.